9-25-2020

KRAS Ubiquitination at Lysine 104 Retains Exchange Factor Regulation by Dynamically Modulating the Conformation of the Interface

Guowei Yin
UNC School of Medicine

Jerry Zhang
UNC School of Medicine

Vinay Nair
University of Texas Health Science Center at Houston

Vinh Truong
University of the Pacific

Angelo Chaia
UNC School of Medicine

See next page for additional authors

Recommended Citation

Authors

Guowei Yin, Jerry Zhang, Vinay Nair, Vinh Truong, Angelo Chaia, Johnny Petela, Joseph S. Harrison, Alemayehu A. Gorfe, and Sharon L. Campbell

iScience

Article

KRAS Ubiquitination at Lysine 104 Retains Exchange Factor Regulation by Dynamically Modulating the Conformation of the Interface
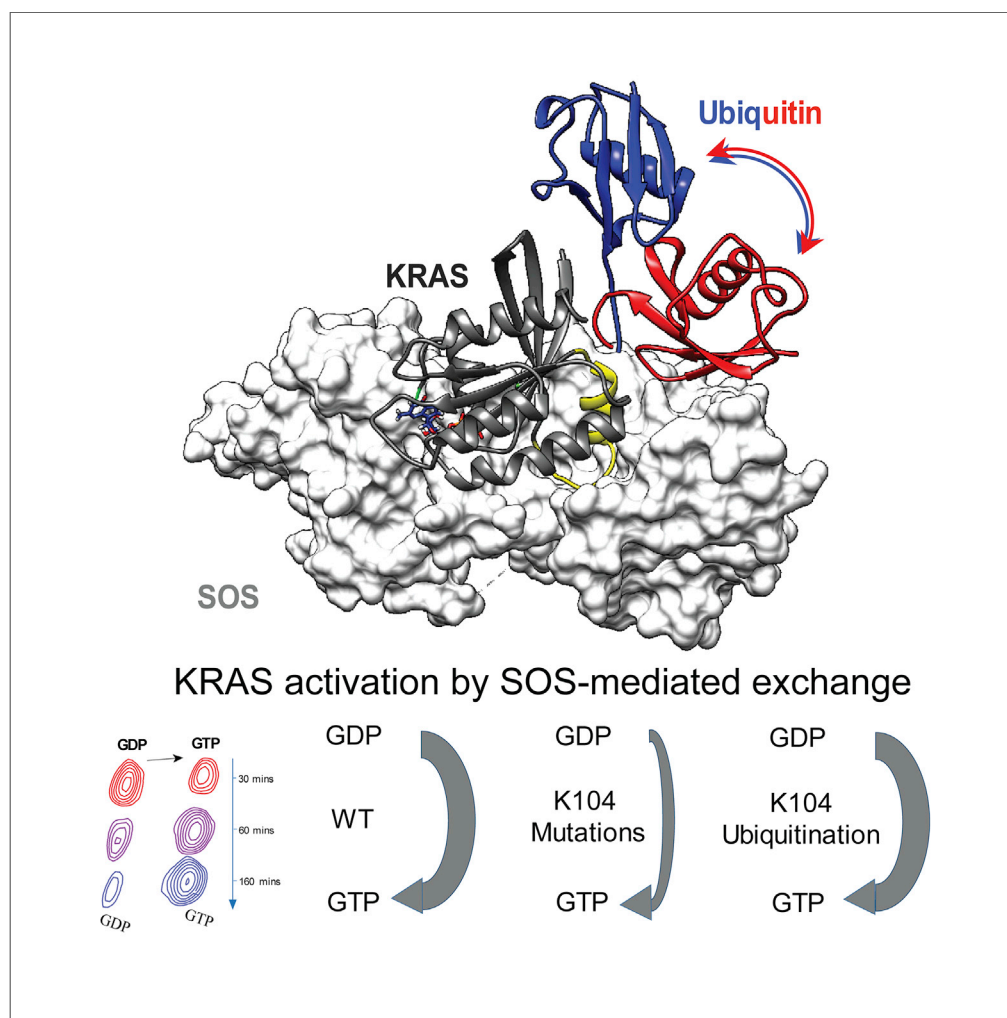
Guowei Yin, Jerry Zhang, Vinay Nair, ..., Joseph Harrison, Alemayehu A. Gorfe, Sharon L. Campbell

campbesl@med.unc.edu

HIGHLIGHTS

Ubiquitination at K104 modulates the conformation and dynamics of Switch II in KRAS

RAS K104 ubiquitination modulates GEF interactions

K104 is a unique site modulating KRAS structure and function

Ubiquitin

KRAS

SOS

KRAS activation by SOS-mediated exchange

GDP → GTP
30 mins
60 mins
160 mins
GDP   GTP

GDP	GDP	GDP
WT	K104 Mutations	K104 Ubiquitination
GTP	GTP	GTP

Article

KRAS Ubiquitination at Lysine 104 Retains Exchange Factor Regulation by Dynamically Modulating the Conformation of the Interface

Guowei Yin,[1,2,7] Jerry Zhang,[1,7] Vinay Nair,[4,5] Vinh Truong,[6] Angelo Chaia,[1] Johnny Petela,[1] Joseph Harrison,[1,6] Alemayehu A. Gorfe,[4,5] and Sharon L. Campbell[1,3,8,*]

SUMMARY

RAS proteins function as highly regulated molecular switches that control cellular growth. In addition to regulatory proteins, RAS undergoes a number of post-translational modifications (PTMs) that regulate its activity. Lysine 104, a hot spot for multiple PTMs, is a highly conserved residue that forms key interactions that stabilize the RAS helix-2(H2)/helix-3(H3) interface. Mutation at 104 attenuates interaction with guanine nucleotide exchange factors (GEFs), whereas ubiquitination at lysine 104 retains GEF regulation. To elucidate how ubiquitination modulates RAS function, we generated monoubiquitinated KRAS at 104 using chemical biology approaches and conducted biochemical, NMR, and computational analyses. We find that ubiquitination promotes a new dynamic interaction network and alters RAS conformational dynamics to retain GEF function. These findings reveal a mechanism by which ubiquitination can regulate protein function.

INTRODUCTION

KRAS is the most frequently mutated oncogene in human cancer, with mutations most prevalent in lung, colorectal, and pancreatic cancers (Waters and Der, 2018). Although inhibitors that target a cysteine 12 oncogenic mutant of KRAS are now in phase 1 clinical trials, inhibitors that target the most prevalent KRAS mutations have yet to be identified (Hansen et al., 2018; Janes et al., 2018). As such, identification of novel regulatory mechanisms may facilitate development of anti-KRAS drugs and treatment options (Cox et al., 2014).

RAS proteins function as binary on-off molecular switches that cycle between inactive GDP-bound and active GTP-bound states and transduce signals through multiple pathways to regulate cellular growth. Nucleotide cycling requires the action of regulatory proteins. In the unstimulated cell, RAS proteins are populated in their inactive GDP-bound state. However, in response to growth-stimulatory signals, guanine nucleotide exchange factors (GEFs) co-localize and activate RAS by facilitating exchange of GDP for GTP. Inactivation is achieved through GTPase-activating proteins (GAPs) that bind to GTP-bound RAS and promote GTP hydrolysis (Geyer and Wittinghofer, 1997; Vigil et al., 2010). RAS contains two dynamic regions termed switch I (SWI; residues 30–37) and switch II (SWII; residues 60–76 with 66–74 corresponding to H2). These switch regions populate distinct conformations when the protein is bound to GDP versus GTP. Effectors and GAP proteins recognize specific conformations of the switch regions and bind with preferential affinity to the active GTP-bound state. Activated GTP-bound RAS can interact with multiple effectors (e.g., RAF kinase, RAL exchange factors, Phosphoinositol 3-Kinase [PI3K], the RAC-selective GEF TIAM1, phospholipase C, NORE1) to promote downstream signaling pathways that control cell growth, differentiation, and apoptosis (Stephen et al., 2014).

Post-translational modifications (PTMs) within the hypervariable carboxyl-terminal domain of RAS are critical for membrane localization and RAS activation (Ahearn et al., 2011). However, less well characterized are PTMs in the core G-domain. These include distinct lysine modifications, such as acetylation, ubiquitination, and most recently methylation (Ahearn et al., 2011; Yoshino et al., 2019). Notably, KRAS monoubiquitination at lysine 147 up-regulates RAS activity, signaling, and tumorigenesis (Baker et al., 2013a; Sasaki et al., 2011). In contrast, monoubiquitination at a minor site, lysine 104 (Sasaki et al., 2011), does not alter the

intrinsic biochemical properties or regulation by GEFs and GAPs (Baker et al., 2013b). Lysine 104 is proximal to the GEF binding surface and can also undergo acetylation, yet the consequence of this modification on RAS activity is controversial. Lysine 104 acetylation (Ac-K104) was initially reported to disrupt activation by GEFs and result in down-regulation of KRAS G12V-driven effector signaling and growth transformation in NIH3T3cells (Yang et al., 2012). These studies were conducted in the context of a KRAS K104Q mutation, which was introduced to mimic constitutive acetylation. However, KRAS K104Q was later shown to have a small yet compensatory GEF/GAP defect (Yin et al., 2017), consistent with findings that KRAS G12V/K104Q retains steady-state GTP-bound levels and the ability of the oncogenic KRAS G12V mutant to cause morphologic transformation of NIH 3T3 mouse fibroblasts (Yin et al., 2017). The differential downstream signaling capabilities of KRAS G12V, K104Q in NIH3T3cells by two distinct groups suggests context dependence associated with this KRAS variant. Notably, KRAS acetylated at lysine 104 *in vitro* using genetic expansion approaches was found to retain GEF regulation (Knyphausen et al., 2016). Hence in this context, K104Q does not serve as an acetylation mimetic.

Lysine 104 appears to be a hot spot for RAS PTMs. This residue plays a key role in regulating SWII conformation, as it forms stabilizing contacts with R73 and G75 in H2. We have previously shown that the K104Q mutation disrupts these electrostatic interactions and causes partial unfolding at this helical interface, resulting in a partial defect in GEF and GAP interactions. To delineate how GEF interactions are retained upon disruption of this electrostatic interaction by ubiquitination, we employed structural, computational, and biochemical approaches. Using real-time NMR, we find the ubiquitination at K104 retains GEF-mediated GDP-GTP exchange, in contrast to mutations at this position (Yin et al., 2017). However, our NMR data indicate that ubiquitination at lysine 104 causes partial disruption of the H2/H3 interface, similar to the K104Q mutation. We next conducted unbiased Rosetta modeling and observed that ubiquitin samples multiple orientations and forms transient contacts with the end of H2 in RAS. We further assessed the conformation and dynamic properties of monoubiquitinated RAS at 104 (mUbKRAS^{104}) using NMR and MD simulations and observe that ubiquitin transiently interacts with H2 and loop 7 to promote formation of a new contact between D69 and R102. This in turn, reduces RAS dynamics, stabilizes the H2/H3 interface, and facilitates GEF binding. Consistent with these predictions, addition of trimethylamine-N-oxide (TMAO) as a cosolute (Su et al., 2017), stabilizes this interface and restores GEF-mediated nucleotide exchange for lysine 104 mutations. Taken together, our findings uncover a novel mechanism of protein regulation by monoubiquitination whereby ubiquitin conjugation dynamically modulates protein recognition.

RESULTS

Monoubiquitination of KRAS at 104 Retains Regulatory and Effector Interactions

The side chain of lysine 104 in KRAS-GDP (PDB 4LPK) forms key interactions with the backbone carbonyl group of R73 and G75 in H2. This interface lies in close proximity to residues R102 and V103, which make direct contacts with the GEF, Son of Sevenless (SOS) (PDB: 1NVW) (Margarit et al., 2003) (Figures 1D and 1E), which plays a key role in RAS activation. Lysine 104 in RAS contacts SWII. These contacts appear key for stabilizing the H2/H3 interface as mutations (K104A, K104Q, K104R, K104C) at this position perturb SOS regulation (Yin et al., 2017) (Table S1, adapted from Yin et al., 2017). In contrast to mutations at 104, mUbKRAS^{104}, generated by conjugating ubiquitin to a RAS K104C variant using disulfide chemistry, retains both SOS- and GAP-mediated regulation (Baker et al., 2013b). The KRAS K104C mutant mUbKRAS^{104} retains thermal stability and the global fold of WT RAS, whereas the K104C mutant shows defects in GEF regulation due to loss of contacts with Switch II (Baker et al., 2013b). To better characterize SOS-mediated guanine nucleotide exchange of mUbKRAS^{104}, we applied real-time NMR. This approach has been used to assay the kinetics of guanine nucleotide exchange by quantitatively monitoring nucleotide-dependent changes in peak intensity and is not complicated by alterations in exchange due to introduction of guanine nucleotide fluorophores (Smith et al., 2015). We then incubated unmodified and monoubiquitinated ^{15}N-enriched KRAS-GDP with native GTP and the SOS catalytic domain (SOS^{cat}) and collected a series of ^{1}H-^{15}N 2D NMR heteronuclear single quantum coherence (HSQC) spectra as a function of time (Figure 1). Two-dimensional ^{1}H-^{15}N HSQC spectra allow for the detection of protons directly bonded to a ^{15}N nucleus, including both backbone and side-chain resonances. Because an NH resonance can be detected for every residue with the exception of proline, the spectrum contains a "fingerprint" of the protein backbone. Upon the addition of GTP and SOS, new peaks corresponding to the GTP-bound state appear. The time course of GDP- and GTP-dependent resonance changes can be fit to obtain nucleotide exchange rate. Depicted in Figure 1B are NH resonances associated with S118 and S145. These peaks are well resolved and sensitive to
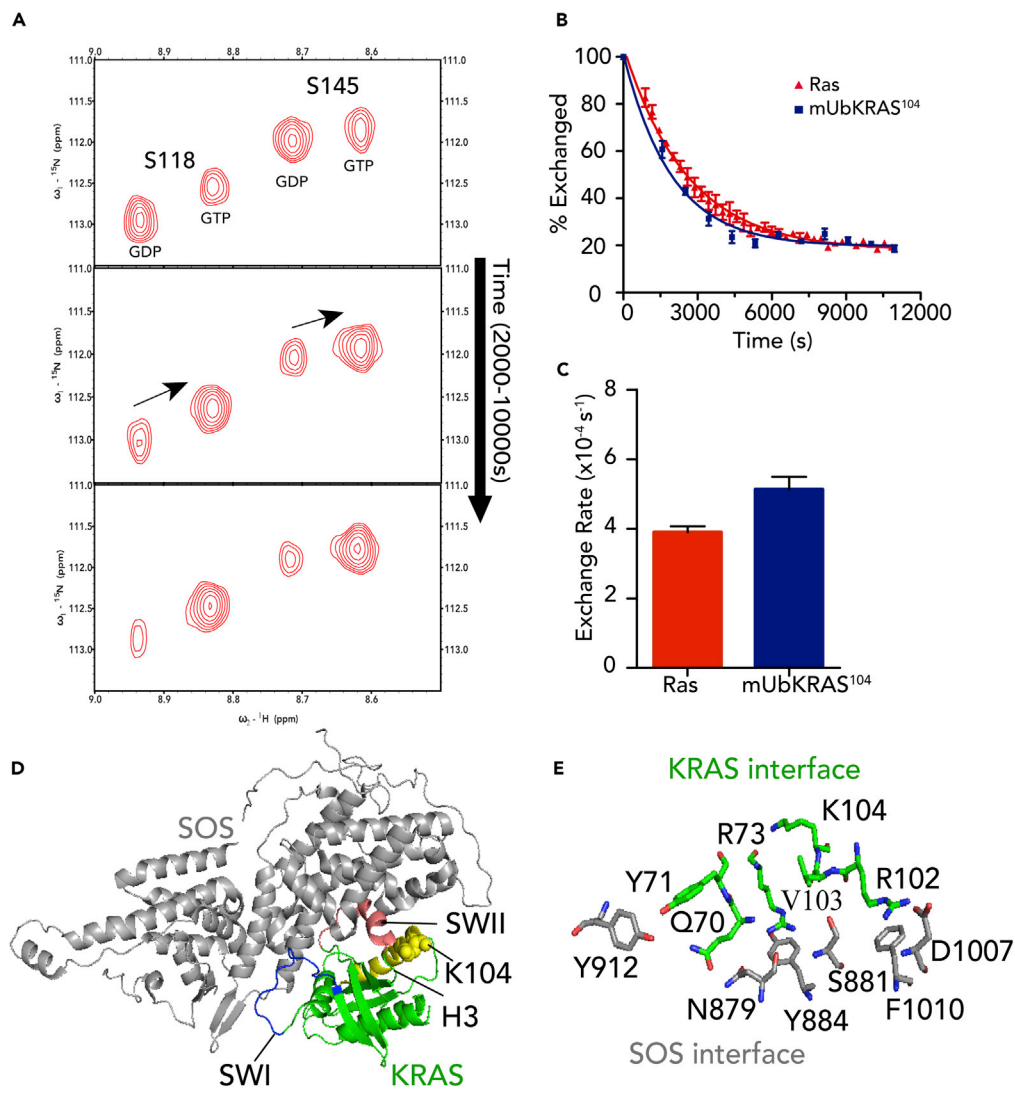
Figure 1. mUbKRAS^{104} Retains Sensitivity to SOS-Mediated Guanine Nucleotide Exchange

(A) Nucleotide exchange rate of WT and mUbKRAS^{104} was determined using real-time NMR. ^{1}H-^{15}N HSQC of ^{15}N-enriched RAS in the presence of the GEF catalytic domain of SOS (SOS^{cat}) was used to monitor amide peaks associated with either the GTP- or GDP-bound state of KRAS. Zoom of HSQC highlighting change over time of S118 and S145 NH resonances resulting from exchange of GDP for GTP. WT KRAS and mUbKRAS^{104} bound to GDP (150 µM) incubated with excess GTP in the presence of SOS^{cat} at a 1,700:1 ratio of RAS to SOS^{cat}. SOS-mediated exchange rates for WT and mUbKRAS^{104} were measured by real-time ^{1}H-^{15}N HSQC NMR over a period of 3 h. Experiments were conducted on a Bruker Avance 850 MHz NMR spectrometer at 20°C in NMR buffer (20 mM Tris-Maleate, 50 mM NaCl, 5 mM MgCl$_2$ pH 7.0).

(B) The percent exchange of GDP for GTP was determined by GDP intensity/(GDP + GTP intensity) for each spectra with respect to time of acquisition. Results were fitted to a single-phase dissociation decay. The errors were determined by SE of the duplicate.

(C) Quantification of relative nucleotide exchange rates. mUbKRAS^{104} shows slightly higher rates of nucleotide exchange relative to WT KRAS. Results are reported as rates of exchange $\pm$SE (n = 2).

(D) Ribbon diagram highlighting the RAS-SOS interface (PDB:1NVW). KRAS is shown in green, SWI in blue, SWII in red, and the K104 side chain in yellow.

(E) Zoom of the RAS-SOS interface highlighting residues proximal to K104 that contribute to complex formation.

GDP-GTP exchange. The GDP/GTP ratio was plotted as a function of time (Figure 1A) and fitted by exponential decay to determine the exchange rate (Figure 1B). Similar to our previous observation using fluorescence-based approaches, monoubiquitination at position 104 retains SOS-mediated GDP-GTP exchange (Figure 1C).

To assess whether binding of RAS to a key downstream effector was altered by KRAS monoubiquitination at 104, we compared the relative binding affinity of GMPPNP-bound mUbKRAS[104] and WT RAS with the RAF kinase. Using a fluorescence-based assay monitoring Mant-GMPPNP dissociation as a function of CRAF RAS-binding domain (RBD) concentration, we observed that mUbKRAS[104] reduces affinity for the CRAF-RBD by ~3-fold relative to WT KRAS (Figure S1).

Monoubiquitination of KRAS-GDP at 104 Causes Structural Perturbations in Helix 2 and Helix 3

To investigate how mUbKRAS[104] retains SOS regulation despite loss of key contacts with SWII, we conducted NMR studies to characterize structural alterations resulting from mUbKRAS[104]. We first assigned 141 of 167 non-proline backbone NH and $C\alpha$ resonances of mUbKRAS[104] bound to Mg^{2+} and GDP by acquiring 3D HNCA triple resonance data on $^{13}C,^{15}N$-enriched protein, using known WT KRAS assignments as a starting point (Yin et al., 2017). A 2D ^1H-^{15}N HSQC spectral overlay of mUbKRAS[104] and WT KRAS bound to GDP is shown in Figure 2A. Inspection of chemical shift differences between KRAS WT and mUbKRAS[104] bound to GDP show that ~40% of the backbone NH peaks undergo chemical shift changes upon ubiquitin modification. Using chemical shift perturbation (CSP) analyses (Figure 2B), the largest CSPs (>0.5 ppm) occur in three regions of the protein: residues proximal to the site of the ubiquitination (positions 103 and 107), residues within SWII, and residues at the C terminus. These findings are consistent with perturbation of contacts between K104, R73, and G75 at the end of SWII. In contrast, a few residues in SWI show mild CSP (35 and 36).

As carbon $C\alpha$ chemical shifts can be used to measure secondary structure propensity (Wishart and Sykes, 1994), we employed chemical shift indexing (CSI) to compare secondary structural differences between mUbKRAS[104] and WT KRAS (Figure 2C). We find that, overall, the secondary structure of mUbKRAS[104] is similar to WT KRAS with the exception of H2 and H3. We calculated the CSI difference between mUbKRAS[104] and WT KRAS. Results shown in Figure 2D indicate a loss of secondary structure for residues 71–75 at the C-terminal end of H2 and alteration of helical content for residues 100–103 in H3 near the mutation site. These secondary structure changes correlate with the large CSP observed for these residues (Figure 2B). Small distortions in secondary structure were also observed in the C-terminal residues (166–167). As the NH peak intensity in the ^1H-^{15}N HSQC spectrum is dependent on the relaxation properties of amides, changes in the peak intensity can be used to assess the changes in local motion. Peak broadening was observed in SWII as well as in the region neighboring the site of modification at 104, including the loop 7 between H3 and β5 (Figure 2E). These observations indicate that ubiquitination of KRAS at 104 not only perturbs H2/H3 secondary structure but also modulates RAS dynamics. Peak broadening was also observed for residues V8 in β1 and T35 and I36 in SWI. The perturbed regions revealed by NMR are highlighted on the 3D structure of WT KRAS bound to GDP [PDB: 4LPK] (Figure 3).

Ubiquitin Forms Dynamic Contacts with Switch II and Stabilizes the RAS-SOS Interface

Our NMR analyses indicate that GDP-bound mUbKRAS[104] perturbs the conformation and dynamics of the RAS H2/H3 interface. Hence, it is unclear how SOS sensitivity is retained despite the observed structural and dynamic perturbations at this key SOS binding interface. To investigate the underlying molecular mechanism, we conducted both Rosetta modeling and MD simulations. Previously, we employed unbiased Rosetta modeling to investigate whether native versus chemical ligation alters conformational sampling of ubiquitin when ligated to KRAS (Saha et al., 2011). We found that chemical ligation of RAS at 147 mimics conformational sampling of the native linkage, as well as the GAP deficiency associated with occlusion effects by ubiquitin modification at K147, consistent with experimental data (Baker et al., 2013a). Using a similar approach, we generated 5,000 models of mUbKRAS[104]. Notably, the lowest 0.1% of scoring models indicates that ubiquitin does not adopt a single conformation when ligated to KRAS at 104 (Figure 4A). These models show little restriction of ubiquitin orientation, with the low scoring models occupying a disc-like shape above KRAS with a diameter of roughly ~65Å (Figure 4A; *right*). Given the ambiguities associated with precision of the Rosetta score function when modeling conjugated ubiquitin, we selected lowest 10% of scoring structures as an approximation for the conformational ensemble of mUbKRAS[104]. We then calculated the contact frequency for each residue of RAS that comes in proximity to ubiquitin (Figure 4B). These analyses indicate that the primary regions of KRAS that ubiquitin contacts are at the end of H2 in SWII, loop 7 between H3 and βI and C terminus. These contacts are consistent with NMR CSPs and peak broadening reported in Figures 2B and 2E, respectively. Residues with significant CSP and broadening at the ubiquitin-KRAS interface of the Rosetta models are highlighted in Figure 4A. We
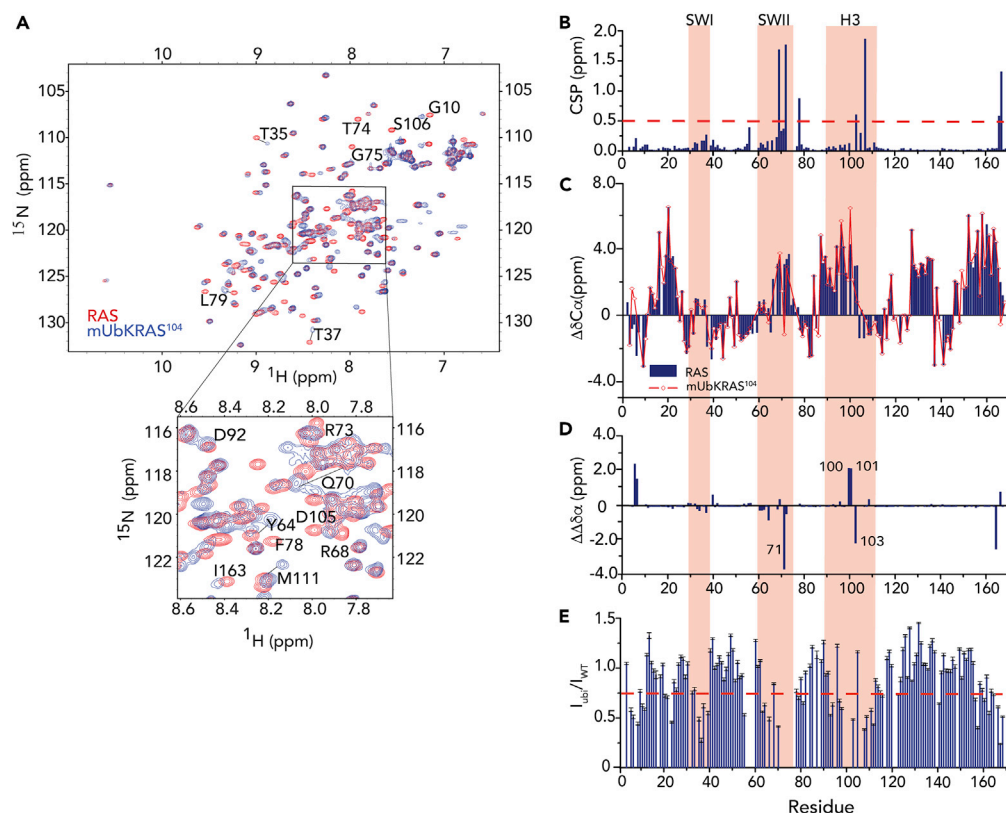
Figure 2. mUbKRAS[104] Alters the Local Conformation and Dynamics of H2 (SWII) and H3

(A) ^{1}H-^{15}N 2D NMR HSQC overlay comparing ^{15}N-enriched mUbKRAS[104] (blue) to WT KRAS (red).

(B) NMR analyses of GDP-bound mUbKRAS[104] relative to WT KRAS shows large chemical shift perturbation (CSPs) in SWII and neighboring residues in H3 but minor changes in β1 within SW1. Chemical shift perturbations were calculated based on weighted average chemical shift (square root of $((\Delta\sigma\,^1H)^2 + (\Delta\sigma\,^{15}N)^2/25)$) of WT and mUbKRAS[104] NH peaks in ^{1}H-^{15}N 2D HSQC NMR spectra of ^{15}N-enriched KRAS-GDP.

(C) Differences in secondary structure between GDP-bound WT KRAS and mUbKRAS[104] determined from Cα and Cβ chemical shift indexing indicate that mUbKRAS[104] perturbs the local conformation surrounding the modification site at 104 in H3 and the H2 (residues 71–74) within SWII.

(D) Difference in chemical shift indexing between GDP-bound mUbKRAS[104] and WT KRAS highlighting perturbations in secondary structure in H3 and the H2 (residues 71–74) in SWII resulting from KRAS monoubiquitination at K104.

(E) Changes in backbone dynamics obtained from 2D ^{1}H-^{15}N HSQC NH peak intensity plot of mUbKRAS[104] compared with WT KRAS. Plot shows pattern of broadening in β1, SWI and II, as well as residues neighboring the modification site at 104. Residues within SWII (residues 73–76) experience significant broadening and were undetectable in the mUbKRAS[104] spectrum. Spectra were recorded using Bruker Avance III 700 and 850 spectrometers at 25°C on a 0.1 mM ^{15}N-enriched samples of GDP-bound KRAS WT and mUbKRAS[104]. The errors were determined by the signal-to-noise ratio of the peak.

also performed the Rosetta modeling of mUbKRAS[104] bound to the SOS[cat] to investigate whether ubiquitin occludes the RAS binding site. We observe that ubiquitin freely samples multiple orientations in the space similar to the mUbKRAS[104] alone and the majority ubiquitin conformers do not share contacts with SOS (Figure S2). Only a minor subset of ubiquitin conformers contact regions (884–909) and (1,019 and 1,021) of SOS, which are not involved in the RAS-SOS interactions. Additionally, those regions of SOS are highly charged and do not possess the typical hydrophobic character that ubiquitin typically needs to interact with the canonical binding site on ubiquitin (Harrison et al., 2016). Collectively, our findings indicate that ubiquitin is capable of making direct contacts with the KRAS at the H2/H3 SOS interface but does not occlude RAS-SOS interactions.

Since the ubiquitin modeling used is primarily a rigid body, this approach is unable to provide information about the dynamics of the protein. Accordingly, we used molecular dynamics simulations to characterize dynamic changes resulting from ubiquitin ligation at position 104. We performed four 1-μs all-atom MD
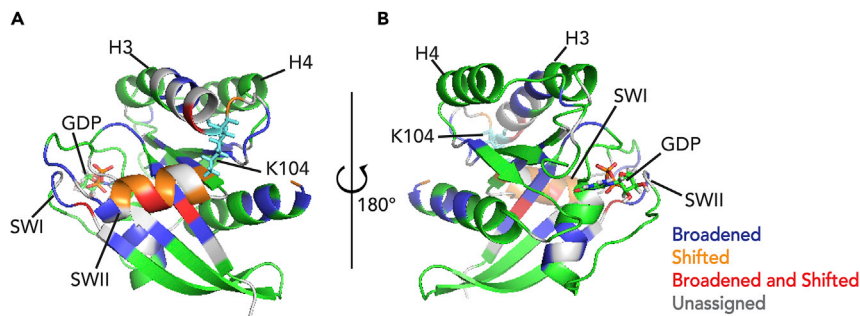
Figure 3. Ribbon Diagram Highlighting NMR Spectral Changes Resulting from mUbKRAS[104]

NMR spectral perturbations (CSP, broadening) resulting from mUbKRAS[104] mapped on the 3D structure of KRAS-GDP (PDB code 4LPK). Resonances associated with residues that display chemical shift changes (CSP >0.5 ppm) are shown in orange, whereas residues that undergo broadening ($I_{mUbKRAS104}/I_{WT}$ < 0.75) are shown in blue. Resonances associated with residues that under both broadening and shifts are shown in red. Unassigned peaks are colored in gray.

simulations, two on GDP-bound mUbKRAS[104] and two on WT KRAS (for reference). As each simulation of mUbKRAS[104] started from two different initial conformations (see Transparent Methods), we checked whether the two simulations converged to a single ensemble using the time evolution of the radius of gyration, the relative orientation of KRAS and ubiquitin, and contacts between KRAS and ubiquitin. As shown in Figure S3, the two simulations do not converge to a single conformation. Rather, they evolved into two distinct ensembles characterized by distinct relative orientations and KRAS-ubiquitin contact profiles. Although there were several attempts at convergence, both the angle and radius gyration plateaued at different values, with one of the simulations sampling a more compact conformation in which ubiquitin forms a larger interface with KRAS. This is illustrated more clearly in the normalized distribution of the angle and radius of gyration using the data in the better-equilibrated last 700 ns of each trajectory (Figure S4). Our observations that the two runs do not sample the same region of configurational space are not entirely unexpected since the large-scale domain motions required for convergence likely occur at timescales longer than a microsecond. Therefore, we checked whether the configurations sampled by the combined trajectory or separately by each simulation are consistent with the wide range of ubiquitin orientations suggested by the proximity analysis of the Rosetta-predicted models and the structural perturbations observed by NMR. As shown in Figure 5A, KRAS-ubiquitin contacts and fluctuations averaged over the two trajectories, but not each trajectory separately, consistent with the data from Rosetta and NMR. This suggests that both trajectories can be regarded as sampling relevant conformations accessible to the complex.

To further analyze the simulation results and evaluate the effect of ubiquitination on KRAS dynamics, we calculated average backbone RMSFs (Figure 5B) and KRAS-ubiquitin residue contacts (Figure 5C) for each simulation. Also shown are RMSFs and contacts averaged over the two trajectories. In one of the simulations, KRAS interacts with ubiquitin primarily via its N terminus, loop 3, and SWII. In the other, ubiquitin interacts with SWII, loop 7, and the C terminus of KRAS (Figures 5C, S3C, and S3D). The combined analysis (average over the two trajectories) indicates that contacts via the N/C termini, loop 3, and loop 7 are transient and occur ~20%–70% of the time, except for E76 (near the C-terminal end of SWII), R164 (C terminus), and K104 (ubiquitination site), which stably persist for >80% of the time. This is consistent with the NMR and Rosetta results described above. Furthermore, from the changes in the average RMSF values per residue, which measure changes in conformational fluctuations due to the ubiquitination, we observe a decrease in SWI and SWII dynamics in trajectory 1. In contrast, the switch regions are, on average, somewhat more dynamic in trajectory 2. The absence of loop 3-ubiquitin interaction in the latter appears to account for the increased dynamics. Ubiquitin stabilized loop 7 in both simulations, which can be explained by the proximity of the loop to the ubiquitination site. Combining the two trajectories, we observe a small but significant dampening of conformational fluctuations in KRAS upon 104 monoubiquitination, especially at SWII, consistent with the broadening observed in the ^{1}H-^{15}N 2D HSQC of mUbKRAS[104] (Figure 2E).

Since the interface between H2 and H3 in KRAS is important for recognition of SOS, we investigated the distances and interaction patterns between the residues in these two helices of mUbKRAS[104] and compared the results with WT KRAS. We observed a mostly conserved pattern of H2-H3 contact (Figure 5D) in the two simulations of mUbKRAS[104] as well as between mUbKRAS[104] and WT KRAS. However, there are some differences. In
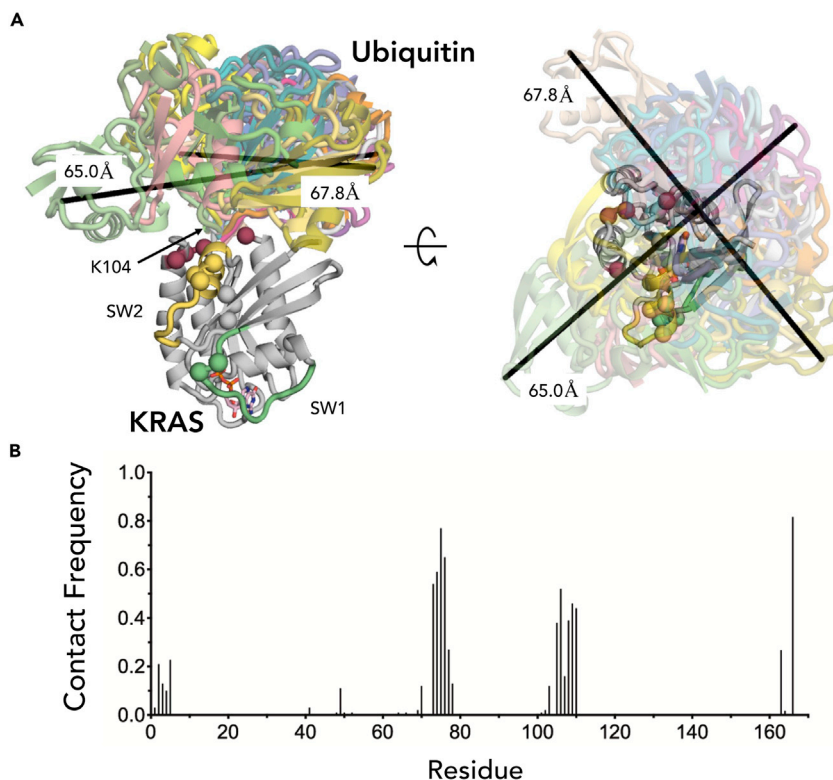
Figure 4. Unbiased Rosetta Modeling of mUbKRAS[104]

Ubiquitin, when ligated to KRAS at 104 in H3, samples multiple orientations and forms transient contacts with RAS at the end of H2 in SWII and loop connecting H3 and H4.

(A) Top 20 Rosetta models of mUbKRAS[104]. mUbKRAS[104] residues displaying CSP greater than 0.5 ppm or peak broadening greater than 50% have Cα carbons shown as a sphere. Purple residues show ubiquitin contacts, whereas gray residues do not contact ubiquitin in the ensemble. Left: side view of the mUbKRAS[104] conformational ensemble; right: view from the top. Ubiquitin occupies roughly 65Å area when conjugated to K104 and with little conformational restriction. SWI residues are colored in green and residues within SW II (residues 61–74) are colored in gold.

(B) Frequency plot of 580 top-scoring Rosetta models that have a KRAS residue within 8Å of ubiquitin by Rosetta Energy Units (~%10 of models). The ubiquitin contact surfaces on RAS mapped by the contact frequency is consistent with peak broadening in the ^{1}H-^{15}N HSQC NMR spectrum of mUbKRAS[104]-GDP.

WT KRAS, the H2/H3 interface is stabilized primarily by interactions involving the side chains of K104, R73, and G75. Ubiquitination at 104 disrupts these interactions. Instead, in both simulations of mUbKRAS[104], we observe a new hydrogen bond between side chains of R102 in H3 and D69 in H2 (Figure 5E), stabilizing the H2/H3 interface and thereby maintaining a site for SOS recognition. In the absence of the D69-R102 hydrogen bond, the H2/H3 interface in mUbKRAS[104] is stabilized by dynamic contacts between the R68 and H95 side chains. Although the loss of interaction involving Lys104 causes some perturbation in the H2/H3 interface (Figure 2D), the helical content of H3 remains intact during the simulations while some loss is observed for H2 compared with WT KRAS by two amino acids in one of the two runs of mUbKRAS[104] (Figure S5). In addition, the helical content of H2 is lost in about 20% of the conformers in simulation 2 of mUbKRAS[104], suggesting a significant impact of ubiquitination on the structure of the H2 in SWII.

TMAO Restores the K104C Sensitivity to SOS-Mediated Guanine Nucleotide Exchange

Our computational and NMR analyses indicate that ubiquitin ligation to KRAS at position 104 retains SOS regulation by stabilizing the H2/H3 interface. To provide further experimental support, we investigated whether osmolytes can similarly restore SOS activity from disruption of the H2/H3 interface by point mutation. We employed the osmolyte, TMAO, as this cosolute can stabilize proteins in solution by enhancing its compact folded conformation even under various denaturing stresses (Guseman et al., 2018; Su et al., 2017). KRAS mutations at position 104, including K104Q, K104C, K104R, and K104A, impair SOS upregulation of RAS activity by disrupting the H2/H3 interface (Baker et al., 2013b; Yin et al., 2017). As such, we
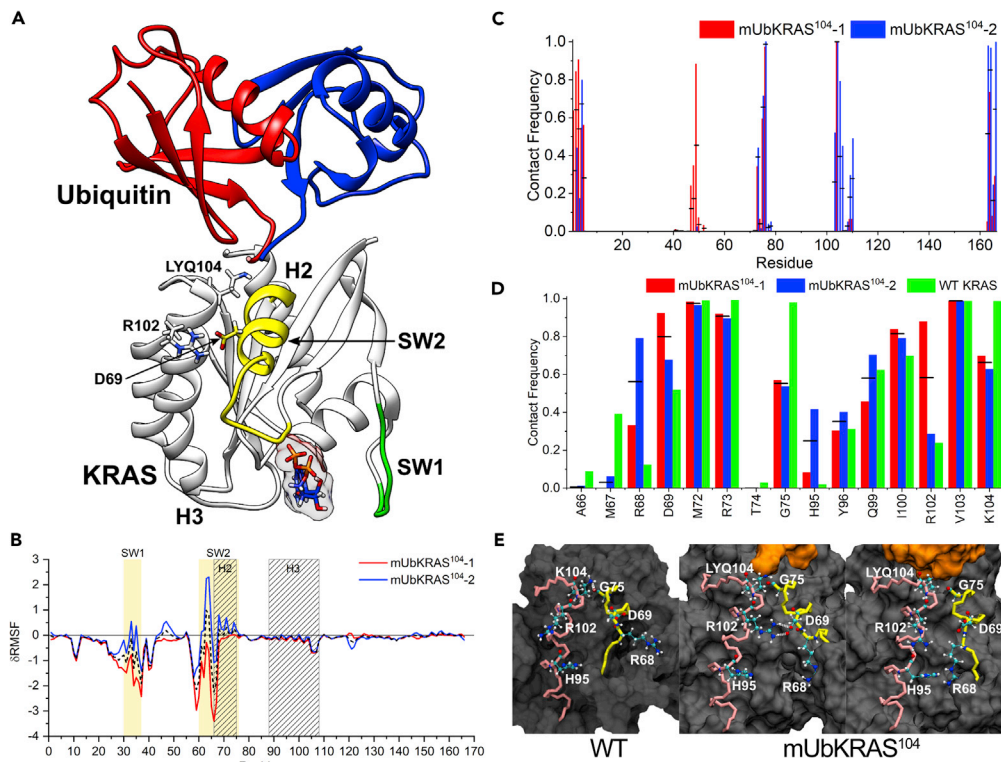
Figure 5. Unbiased Atomistic MD Simulations of mUbKRAS[104] Bound to GDP Suggest that Ubiquitin Forms Dynamic Interactions with the KRAS Switch Regions

(A) The relative orientation of ubiquitin and KRAS derived from two independent MD runs of mUbKRAS[104] bound to GDP. KRAS is shown in gray with SWI and SWII in green and yellow, respectively. Representative structures of ubiquitin from simulation 1 and 2 are depicted in red and blue, respectively. The nucleotide is shown as licorice structure at the bottom of the image.

(B) The difference of residue root-mean-square fluctuations (δRMSF) between WT KRAS and mUbKRAS[104] averaged over the last 700 ns of simulation 1 (red), simulation 2 (blue), and their average (black dashed line). SWI and SWII regions are highlighted in yellow, and H2 and H3 in black slanted lines.

(C) Normalized contact frequencies of KRAS with ubiquitin residues in simulation 1 (red) and 2 (blue) of mUbRAS[104]-GDP.

(D) Normalized frequency of contacts for residues in H2 and H3 in ensembles of mUbKRAS[104] and WT KRAS bound to GDP. In (C) and (D), values averaged over the two simulations are shown as black dashes.

(E) Snapshots between mUbKRAS[104] and WT KRAS bound to GDP highlighting differences in interactions between select H2 (yellow) and H3 (pink) residues. Hydrogen bonds are depicted as white dashes. KRAS and ubiquitin are depicted as black and orange surfaces, respectively.

investigated whether TMAO can stabilize mutational perturbation at the H2/H3 interface and restore SOS activity. As a cysteine mutation at position 104 was used to generate a disulfide linkage between RAS and ubiquitin, we investigated the effects of TMAO on SOS-mediated KRAS[104C] guanine nucleotide dissociation. For these experiments, we loaded KRAS[K104C] with MANT-GDP and determined the rate of MANT-GDP nucleotide dissociation in the absence and presence of SOS[cat]. Consistent with our previous findings that mutations at 104 perturb SOS regulation, KRAS[K104C] reduces SOS-mediated nucleotide dissociation (Figure 6). However, the presence of 500 mM TMAO significantly restores the SOS-mediated GDP dissociation rate. These data indicate that, like ubiquitination, TMAO can partially restore SOS activity by stabilizing RAS conformation and dynamics.

DISCUSSION

Post-translational modifications within the G-domain of RAS proteins present an additional layer of complexity in modulation of RAS activity and may provide novel avenues to target RAS-driven tumorigenesis (Ahearn et al., 2018, 2011). To date, PTMs such as ubiquitination, acetylation ,and methylation have been identified in G domain of RAS at multiple sites, including K104, K117, and K147 (Ahearn et al., 2018). The modulatory effects of PTMs on
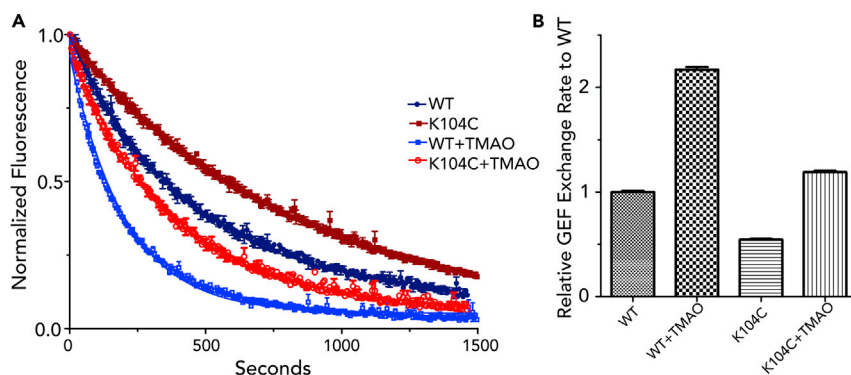
Figure 6. The Osmolyte TMAO Enhances SOS^cat-mediated RAS-GDP Nucleotide Dissociation for WT and KRAS^K104C

(A) The relative rates of SOS-mediated GDP dissociation for WT KRAS and KRAS^K104C in the absence and presence of the osmolyte TMAO were measured using a fluorescence-based assay.

(B) Quantification of SOS-mediated GDP dissociation. KRAS^K104C shows reduced SOS^cat-mediated GDP dissociation relative to WT KRAS. Addition of 0.5 M Trimethylamine N-Oxide (TMAO) stimulates SOS-mediated nucleotide exchange for both WT and KRAS^K104C. All the measurements were performed in duplicate; results are the mean $\pm$ SD (n = 2).

RAS are dependent on the site and type (Ahearn et al., 2018). Although a number of PTMs in RAS have been reported, deciphering molecular mechanisms associated with modulation of RAS activity and tumorigenesis are often hampered by limited methods available to authentically install the type of PTM at the specific site of RAS both *in vivo* and *in vitro*. As such, proper installation of the PTM on RAS and characterization at the molecular level will aid in understanding the functional and structural consequences. Previously we found that ubiquitination at K147 of KRAS promotes activation of RAS by abrogating GAP-mediated hydrolysis (Baker et al., 2013a). We also observed that ubiquitination of KRAS at 104 retains SOS regulation. In contrast, mutations at this site disrupt SOS-mediated guanine dissociation (Baker et al., 2013b). In characterizing the effects of mUbKRAS^104, we uncovered a novel mechanism by which conjugating ubiquitin to RAS modulates RAS dynamics and RAS/GEF interactions.

By employing real-time NMR, we find that mUbKRAS^104 retains SOS-mediated GDP-GTP exchange similar to WT KRAS, consistent with our previous findings (Baker et al., 2013b). Lysine 104 lies in H3. The K104 side chain interacts with backbone carbonyl oxygens of R73 and G75 in H2 and is important for maintaining the integrity of H2 in SWII. Moreover H2 and H3 provide key contacts for SOS recognition based on crystal structures of RAS proteins bound to SOS1^cat (PDB codes 1BKD, 1NVW, and 1XD2) (Margarit et al., 2003; Sondermann et al., 2004). Specifically, R102 in H3 makes contacts with Phe1010 and Asp1007 in SOS^cat. Valine103, adjacent to the modification site, interacts with Ser881 in SOS^cat. Moreover, RAS residues Gln70, Tyr71, and R73 at the end of H2 form additional interactions with SOS^cat (Figures 1D and 1E) (Hall et al., 2001). Therefore, the structural integrity of the H2/H3 interface is important for SOS recognition. Consistent with these observations, mutations at 104 perturb SOS-mediated nucleotide exchange. NMR analyses indicate that ubiquitination at 104 perturbs regions in H2 and H3, including residues 70–78 and residues 100–108. However, although ubiquitination results in loss of these native interactions, new interactions are generated. Rosetta modeling shows that ubiquitin, when ligated at 104 to RAS, can sample conformations in proximity to regions that show NMR perturbations. This observation was further corroborated by MD simulations, which yielded two major ensembles of mUbKRAS^104 conformers wherein the ubiquitin-KRAS interface involves both H2 and H3.

We also set out to quantitatively assess changes in dynamic properties of SWII at atomic resolution using NMR spin relaxation experiments, but the sample stability was not sufficient to carry out the intensity modulation experiments for measuring the relaxation rates. In lieu of quantifying mUbKRAS^104 dynamics by NMR, we employed MD simulations. The MD simulations complement our experimental data and show a reduction in RMSD fluctuations (Figure 5B), consistent with the NMR peak broadening observed in SWI and SWII (Figure 2E). For the majority of the mUbKRAS^104 conformers, the H2/H3 interface is stabilized through altered dynamics of H2 and formation of a dynamic interaction network that compensates for loss of native H2-H3 interactions. The D69-R102 interaction observed in some crystal structures (Johnson et al., 2019) and previous simulations (Rambahal, 2013) stabilizes a portion of SWII in a more GTP-like conformation in which H2 orients toward H3. Given these observations, we analyzed the existing PDB structure of

RAS proteins for D69 and R102 interactions and found hydrogen bonds in 20.4% of the GDP-bound structures and 46.1% of the GTP-bound structures (Table S2). This is consistent with peak broadening observed at the end of H2 and residues proximal to K104 (Figure 2E). Moreover, our findings that addition of the osmolyte TMAO restores SOS deficiency caused by mutation at 104 provides additional evidence that stabilizing interactions can compensate for loss of 104 contacts with H2. To date, TMAO has not been reported in the studies of RAS. TMAO is a natural osmolyte that stabilizes a wide spectrum of proteins against hydrostatic pressure, heat, and denaturing agents like urea (Walker et al., 2019). A widely accepted theory is that TMAO stabilizes proteins by increasing the free energy of the unfolded state through solvent exclusion and hydrogen bonding of water and thus shifts the equilibrium toward the native state (Ma et al., 2014). In a recent paper, TMAO was postulated to stabilize charge interactions between residues (Su et al., 2017).

Our computational analyses indicate that ubiquitin does not dock or form strong molecular interactions that anchor ubiquitin at the RAS surface, yet forms transient interactions with RAS and alters RAS dynamics in the proximity of the KRAS H2-H3 interface. Consistently, we have previously titrated ^{15}N-enriched KRAS with a large excess of free ubiquitin and did not observe the significant interactions by NMR. Hence, ubiquitin modulates RAS structure and dynamics, by dynamically sampling the RAS surface. This novel mechanism of RAS regulation adds to accumulating evidence that dynamic protein complexes (Hopper and Robinson, 2014; Lobingier et al., 2017) together with inherent protein dynamics, play important roles in modulating multiple cellular processes such as signaling pathways, chaperon-assistant folding and transcriptional regulation (Csizmok et al., 2016; Sandikci et al., 2013; Stein et al., 2009; Tompa et al., 2015).

Furthermore, although ubiquitin conjugation to RAS at 104 dynamically samples multiple orientations with a large amplitude at the KRAS surface, our Rosetta modeling (Figure S2) and MD simulations (Figure S6) indicate that the ubiquitin does not occlude the RAS-SOS interface. Therefore, our finding that the ubiquitin modulates the dynamics of SWII to stabilize the H2/H3 interface to restore SOS-mediated activation represents a new mechanism for modulation of RAS signaling. It is worth noting that this mechanism has been proposed in a computational study for kinases (Ball et al., 2016). Ubiquitin PTMs are generally thought to function as recognition elements that bind ubiquitin recognition motifs. Although it is unclear whether mUbKRAS^{104} promotes new interactions in this manner, our data indicate that ubiquitin conjugation can alter the conformational ensemble of a dynamic proteins. This represents a paradigm for ubiquitin signaling and provides a potential mechanism for how ubiquitin conjugation can alter protein function.

Lysine 104 of KRAS is a hotspot for PTMs; however, the physiological roles of lysine modifications at this site and interplay between the different PTMs are unclear. Moreover, investigation of the interplay between the different PTMs is needed. As monoubiquitination and acetylation are mutually exclusive, mechanisms may exist to choose between different modifications at this site in response to changes in the cellular environment or signaling events. It will be interesting to characterize these two PTMs at K104 in the context of the oncogenic mutations of KRAS and the potential interplay. Our findings indicate that RAS lysine 104 monoubiquitination does not alter intrinsic or regulator-mediated biochemical function. Therefore, the biological role of ubiquitination at this site is still unclear. Ubiquitination at K104 may create a new docking site to promote or interfere with RAS interacting proteins or modulate other lysine modifications. However, identification of enzymes that control RAS ubiquitination at this site is needed to dissect the role of this modification and assess whether this mechanism of regulation presents new opportunities to target aberrant RAS signaling and tumorigenesis.

METHODS

All methods can be found in the accompanying Transparent Methods supplemental file.

SUPPLEMENTAL INFORMATION

Supplemental Information can be found online at https://doi.org/10.1016/j.isci.2020.101448.

ACKNOWLEDGMENTS

REFERENCES

Ahearn, I., Zhou, M., and Philips, M.R. (2018). Posttranslational modifications of RAS proteins. Cold Spring Harb. Perspect. Med. *8*, a031484.

Ahearn, I.M., Haigis, K., Bar-Sagi, D., and Philips, M.R. (2011). Regulating the regulator: post-translational modification of RAS. Nat. Rev. Mol. Cell Biol. *13*, 39–51.

Baker, R., Lewis, S.M., Sasaki, A.T., Wilkerson, E.M., Locasale, J.W., Cantley, L.C., Kuhlman, B., Dohlman, H.G., and Campbell, S.L. (2013a). Site-specific monoubiquitination activates Ras by impeding GTPase-activating protein function. Nat. Struct. Mol. Biol. *20*, 46–52.

Baker, R., Wilkerson, E.M., Sumita, K., Isom, D.G., Sasaki, A.T., Dohlman, H.G., and Campbell, S.L. (2013b). Differences in the regulation of K-Ras and H-Ras isoforms by monoubiquitination. J. Biol. Chem. *288*, 36856–36862.

Ball, K.A., Johnson, J.R., Lewinski, M.K., Guatelli, J., Verschueren, E., Krogan, N.J., and Jacobson, M.P. (2016). Non-degradative ubiquitination of protein kinases. PLoS Comput. Biol. *12*, e1004898.

Cox, A.D., Fesik, S.W., Kimmelman, A.C., Luo, J., and Der, C.J. (2014). Drugging the undruggable RAS: Mission possible? Nat. Rev. Drug Discov. *13*, 828–851.

Csizmok, V., Follis, A.V., Kriwacki, R.W., and Forman-Kay, J.D. (2016). Dynamic protein interaction networks and new structural paradigms in signaling. Chem. Rev. *116*, 6424–6462.

Geyer, M., and Wittinghofer, A. (1997). GEFs, GAPs, GDIs and effectors: taking a closer (3D) look at the regulation of Ras-related GTP-binding proteins. Curr. Opin. Struct. Biol. *7*, 786–792.

Guseman, A.J., Perez Goncalves, G.M., Speer, S.L., Young, G.B., and Pielak, G.J. (2018). Protein shape modulates crowding effects. Proc. Natl. Acad. Sci. U S A *115*, 10965–10970.

Hall, B.E., Yang, S.S., Boriack-Sjodin, P.A., Kuriyan, J., and Bar-Sagi, D. (2001). Structure-based mutagenesis reveals distinct functions for Ras switch 1 and switch 2 in Sos-catalyzed guanine nucleotide exchange. J. Biol. Chem. *276*, 27629–27637.

Hansen, R., Peters, U., Babbar, A., Chen, Y., Feng, J., Janes, M.R., Li, L.-S., Ren, P., Liu, Y., and Zarrinkar, P.P. (2018). The reactivity-driven biochemical mechanism of covalent KRASG12C inhibitors. Nat. Struct. Mol. Biol. *25*, 454–462.

Harrison, J.S., Jacobs, T.M., Houlihan, K., Van Doorslaer, K., and Kuhlman, B. (2016). UbSRD: the ubiquitin structural relational database. J. Mol. Biol. *428*, 679–687.

Hopper, J.T.S., and Robinson, C.V. (2014). Mass spectrometry quantifies protein interactions–from molecular chaperones to membrane porins. Angew. Chem. Int. Ed. *53*, 14002–14015.

Janes, M.R., Zhang, J., Li, L.-S., Hansen, R., Peters, U., Guo, X., Chen, Y., Babbar, A., Firdaus, S.J., Darjania, L., et al. (2018). Targeting KRAS mutant cancers with a covalent G12C-specific inhibitor. Cell *172*, 578–589.e17.

Johnson, C.W., Lin, Y.-J., Reid, D., Parker, J., Pavlopoulos, S., Dischinger, P., Graveel, C., Aguirre, A.J., Steensma, M., Haigis, K.M., et al. (2019). Isoform-specific destabilization of the active site reveals a molecular mechanism of intrinsic activation of KRas G13D. Cell Rep. *28*, 1538–1550.e7.

Knyphausen, P., Lang, F., Baldus, L., Extra, A., and Lammers, M. (2016). Insights into K-Ras 4B regulation by post-translational lysine acetylation. Biol. Chem. *397*, 1071–1085.

Lobingier, B.T., Hüttenhain, R., Eichel, K., Miller, K.B., Ting, A.Y., von Zastrow, M., and Krogan, N.J. (2017). An approach to spatiotemporally resolve protein interaction networks in living cells. Cell *169*, 350–360.e12.

Ma, J., Pazos, I.M., and Gai, F. (2014). Microscopic insights into the protein-stabilizing effect of trimethylamine N-oxide (TMAO). Proc. Natl. Acad. Sci. U S A *111*, 8476–8481.

Margarit, S.M., Sondermann, H., Hall, B.E., Nagar, B., Hoelz, A., Pirruccello, M., Bar-Sagi, D., and Kuriyan, J. (2003). Structural evidence for feedback activation by Ras.GTP of the Ras-specific nucleotide exchange factor SOS. Cell *112*, 685–695.

Rambahal, N. (2013). Conformational Dynamics of K-RAS and H-RAS Proteins: Is There Functional Specificity at the Catalytic Domain? UT GSBS Dissertations and Theses (Open Access). https://digitalcommons.library.tmc.edu/utgsbs_dissertations/380/.

Saha, A., Lewis, S., Kleiger, G., Kuhlman, B., and Deshaies, R.J. (2011). Essential role for ubiquitin-ubiquitin-conjugating enzyme interaction in ubiquitin discharge from Cdc34 to substrate. Mol. Cell *42*, 75–83.

Sandikci, A., Gloge, F., Martinez, M., Mayer, M.P., Wade, R., Bukau, B., and Kramer, G. (2013). Dynamic enzyme docking to the ribosome coordinates N-terminal processing with polypeptide folding. Nat. Struct. Mol. Biol. *20*, 843–850.

Sasaki, A.T., Carracedo, A., Locasale, J.W., Anastasiou, D., Takeuchi, K., Kahoud, E.R., Haviv, S., Asara, J.M., Pandolfi, P.P., and Cantley, L.C. (2011). Ubiquitination of K-Ras enhances activation and facilitates binding to select downstream effectors. Sci. Signal. *4*, ra13.

Smith, M.J., Marshall, C.B., Theillet, F.-X., Binolfi, A., Selenko, P., and Ikura, M. (2015). Real-time NMR monitoring of biological activities in complex physiological environments. Curr. Opin. Struct. Biol. *32*, 39–47.

Sondermann, H., Soisson, S.M., Boykevisch, S., Yang, S.-S., Bar-Sagi, D., and Kuriyan, J. (2004). Structural analysis of autoinhibition in the Ras activator son of sevenless. Cell *119*, 393–405.

Stein, A., Pache, R.A., Bernadó, P., Pons, M., and Aloy, P. (2009). Dynamic interactions of proteins in complex networks: a more structured view. FEBS J. *276*, 5390–5405.

Stephen, A.G., Esposito, D., Bagni, R.K., and McCormick, F. (2014). Dragging ras back in the ring. Cancer Cell *25*, 272–281.

Su, Z., Mahmoudinobar, F., and Dias, C.L. (2017). Effects of trimethylamine-N-oxide on the conformation of peptides and its implications for proteins. Phys. Rev. Lett. *119*, 108102.

Tompa, P., Schad, E., Tantos, A., and Kalmar, L. (2015). Intrinsically disordered proteins: emerging interaction specialists. Curr. Opin. Struct. Biol. *35*, 49–59.

Vigil, D., Cherfils, J., Rossman, K.L., and Der, C.J. (2010). Ras superfamily GEFs and GAPs: validated and tractable targets for cancer therapy? Nat. Rev. Cancer *10*, 842–857.

Walker, E.J., Bettinger, J.Q., Welle, K.A., Hryhorenko, J.R., and Ghaemmaghami, S. (2019). Global analysis of methionine oxidation provides a census of folding stabilities for the human proteome. Proc. Natl. Acad. Sci. U S A *116*, 6081–6090.

Waters, A.M., and Der, C.J. (2018). KRAS: the critical driver and therapeutic target for pancreatic cancer. Cold Spring Harb. Perspect. Med. *8*, a031435.

Wishart, D.S., and Sykes, B.D. (1994). The 13C chemical-shift index: a simple method for the identification of protein secondary structure using 13C chemical-shift data. J. Biomol. NMR *4*, 171–180.

Yang, M.H., Nickerson, S., Kim, E.T., Liot, C., Laurent, G., Spang, R., Philips, M.R., Shan, Y., Shaw, D.E., Bar-Sagi, D., et al. (2012). Regulation of RAS oncogenicity by acetylation. Proc. Natl. Acad. Sci. U S A *109*, 10843–10848.

Yin, G., Kistler, S., George, S.D., Kuhlmann, N., Garvey, L., Huynh, M., Bagni, R.K., Lammers, M., Der, C.J., and Campbell, S.L. (2017). A KRAS GTPase K104Q mutant retains downstream signaling by offsetting defects in regulation. J. Biol. Chem. *292*, 4446–4456.

Yoshino, H., Yin, G., Kawaguchi, R., Popov, K.I., Temple, B., Sasaki, M., Kofuji, S., Wolfe, K., Kofuji, K., Okumura, K., et al. (2019). Identification of lysine methylation in the core GTPase domain by GoMADScan. PLoS One *14*, e0219436.

Supplemental Information

KRAS Ubiquitination at Lysine 104 Retains

Exchange Factor Regulation by Dynamically

Modulating the Conformation of the Interface

Guowei Yin, Jerry Zhang, Vinay Nair, Vinh Truong, Angelo Chaia, Johnny Petela, Joseph Harrison, Alemayehu A. Gorfe, and Sharon L. Campbell

Transparent methods for iScience ISCIENCE-D-20-00449R1, *Yin* et al.

Protein Expression and Purification. The human KRAS4B (C118S) cDNA sequence encoding the G-domain (guanine nucleotide binding domain, residues 1-169)) was subcloned into a pET21 vector that adds an N-terminal 6x-histidine tag and a TEV protease cleavage site for expression of recombinant protein in E. coli BL21(DE3) cells (Novagen). Standard site-directed mutagenesis techniques were used to generate KRAS cDNA sequences encoding the K104C missense mutant. The KRAS K104C mutant was verified by DNA sequencing. *E. coli* BL21 (DE3) cells were grown at 37°C in Luria-Bertani (LB) medium supplemented with ampicillin and chloramphenicol until OD600 ~ 0.5. The temperature was then lowered to 18°C, and KRAS expression was induced with 0.5 mM isopropyl-β-D-1-thiogalactopyrano-side (IPTG) after 30 min. The cells were grown for an additional 15 h at 18°C, then harvested, pelleted at 4000 rpm, and resuspended in a lysis buffer (20 mM HEPES, 500 mM NaCl, 1 mM $MgCl_2$, 20 mM imidazole, 5% glycerol (pH 7.75) containing the protease inhibitor Phenylmethanesulfonyl fluoride (ACROS Organics)). Cell lysis was achieved by sonication, and the supernatant isolated by centrifugation at 15,000 rpm. KRAS proteins were then purified using Ni-NTA agarose affinity chromatography (Qiagen). The histidine tag was cleaved during overnight dialysis using TEV protease. KRAS proteins were further purified by size exclusion chromatography using a Sephadex G-75 column. Protein purity >95% was obtained as verified by SDS-PAGE analysis. Full length Ubiquitin G76C was expressed in pQlinkH vector and expressed in *E. coli* BL21(DE3) pLysS cells. The cells were lysed using lysis buffer (30 mM Hepes, 150 mM NaCl, 5mM $MgCl_2$, 10 mM imidazole (pH 8.00) and cOmpleteTM Protease inhibitor cocktail (Sigma Aldrich) and sonicated. Ubiquitin was then purified using nickel affinity chromatography. Tris(2-carboxyethyl)phosphine (TCEP, 2.5 mM) was added to KRAS K104C and Ubiquitin G76C for all purification steps to prevent oxidation. The catalytic domain of human SOS1 (SOS^{cat}, residues 566-1049) (Sondermann et al., 2004) was expressed in a pQlinkH vector (Addgene) and purified as previously described (Baker et al., 2013). The cDNA sequence encoding the isolated RAS-binding domains (RBDs) of human CRAF (51-132) was subcloned in a pET28a bacterial expression vector containing an N-terminal 6x-histidine tag and TEV cleavage site, and subsequently expressed in BL21 (DE3) cells. The CRAF RBD was purified using Ni-NTA affinity chromatography. The N-terminal tag was cleaved using TEV protease. The CRAF-RBD was further purified using size exclusion chromatography (Sephadex G-75) and verified to be >95% pure by SDS-PAGE analysis.

Ligation of Ubiquitin^{G76C} to RAS^{K104C}. The chemical ligation strategy used to link RAS to Ubiquitin^{G76C} was adapted from Baker et al (Baker et al., 2013), using ten–fold excess of Ubiquitin^{G76C} to RAS^{K104C} with dialysis in 50 mM Tris, 50 mM NaCl, 5 mM $MgCl_2$, 10 mM GDP pH 7.85 at 4 °C overnight. The amount of disulfide complex formation was determined by non–reducing SDS–PAGE and considered complete by the absence of unmodified RAS.

Fluorescence based RAS-nucleotide exchange assay. The rate of nucleotide exchange was measured by a fluorescence-based assay using MANT-GDP (BioLog, San Diego, CA) as previously reported (Lenzen et al., 1998). Briefly, MANT-GDP–loaded RAS was added to 1 mL assay buffer (20 mM HEPES, 50 mM NaCl, 5 mM MgCl2, and 100 μM DTPA, pH 7.4) at a final concentration of 1 μM. Nucleotide exchange was initiated by addition of 0.5 mM GDP. In experiments using Trimethylamine N-oxide (TMAO), 0.5 M TMAO was added to the reaction buffer. MANT-GDP dissociation was measured as a change in fluorescence intensity over time (excitation: 365 nm, emission: 435 nm) (LS50B PerkinElmer Luminescence Spectrometer). The fluorescence data was fitted in GraphPad Prism (GraphPad Software, San Diego, CA) to a one-phase exponential decay curve. For SOS-mediated dissociation, 1 μM RAS and 1 μM SOS^{cat} were used. Results are plotted as the mean ± S.E. (n = 2).

Effector binding assay. KRAS was preloaded with MANT-GMPPNP using methods described previously (Yin et al., 2017). Briefly, 1.5 μM MANT-GMPPNP-bound KRAS was incubated with the CRAF-RBD (0.5 - 10 μM) in a buffer containing 20 mM HEPES, 50 mM NaCl, and 5 mM $MgCl_2$ at pH 7.4. Nucleotide dissociation was initiated by the addition of 500 μM of GDP, and the rate of dissociation determined by monitoring the change in fluorescence of the MANT-GMPPNP-loaded protein (excitation and emission wavelengths of 335 and 485 nm, respectively) using a SpectraMax M2 plate reader (Lenzen et al., 1995). Each nucleotide dissociation curve

was fit to a one-phase single exponential to determine k_{obs}. The dissociation rates were plotted against the effector concentrations and fit to determine the equilibrium dissociation constant (K_d).

NMR analyses. For NMR measurements, [^{13}C,^{15}N]-enriched KRAS proteins were exchanged into NMR buffer (20 mM Tris-Maleate (pH 6.5), 40 mM NaCl, 5 mM MgCl$_2$ and 20 µM GDP, 5% D$_2$O). NMR spectra were acquired at 25 °C on Bruker Avance 700 and 850 NMR spectrometers. Two-dimensional ^{1}H–^{15}N HSQC experiments were recorded for both WT and mUbKRAS[104] bound to GDP, with 1024 and 256 complex points in the direct and indirect dimensions, respectively, using 32 scans per increment and a recovery delay of 1.0 s. Spectral widths used were 9803.992 Hz (^{1}H) and 2553.626 (^{15}N) Hz. Spectra were processed and analyzed using NMRPipe (NIDDK, NIH) and NMRFARM Sparky (Lee et al., 2015). Backbone resonance assignments of WT KRAS bound to GDP were previously obtained (Yin et al., 2017). 3D HNCA data then used to obtain assignments for mUbKRAS[104]. 3D HNCA data were recorded on ^{13}C, ^{15}N-labeled mUbKRAS[104] bound to GDP [^{13}C, ^{15}N]-enriched RAS K104C ligated to unlabeled Ubiquitin G76C, 0.4 mM). Cα, N, and HN assignments were obtained by an iterative procedure using the MARS program (Jung and Zweckstetter, 2004) by manual transfer of WT KRAS assignments. Average ^{1}H-^{15}N chemical shift perturbations were calculated according to the square root of $[(\Delta\sigma\ ^{1}H)^2 + (\Delta\sigma\ ^{15}N)^2 /25]$, where $\Delta\sigma\ ^{1}H$ and $\Delta\sigma\ ^{15}N$ are the observed changes in ^{1}H and ^{15}N chemical shifts. For chemical shift indexing (CSI), ΔCα values were calculated by subtracting experimental chemical shifts of Cα from random coil values obtained from the ncIDP server (Tamiola et al., 2010). The value of ΔCα was used to predict RAS secondary structure.

Real-time NMR data were acquired using a strategy described by Mazhab-Jafari et al (Mazhab-Jafari et al., 2010). Two dimensional ^{1}H-^{15}N HSQC experiments (parameters previously described in NMR analyses) were set up sequentially on either a Bruker Avance III 700 or 850 MHz NMR spectrometer at 20°C. Nucleotide exchange experiments were conducted by exchanging ^{15}N-enriched, GDP-bound KRAS into NMR exchange buffer (20 mM Tris-Maleate, 50 mM NaCl, 5 mM MgCl$_2$, pH 7.0). Excess GTP at a ratio of GTP:KRAS 15:1 and SOS^{cat}:KRAS 1:1700 was added before initiating HSQC experiments. A series of HSQC experiments were queued over a span of 3 hours to obtain a several 2D HSQC spectra (4 scans per increment).

Peak changes associated with either the RAS-GDP and GTP-bound state were tracked over time. The peak intensity for residues S118, S145 for both GTP and GDP peaks of KRAS was quantified using Topspin spectra analysis. The percent exchanged was determined by GDP intensity/(GDP+GTP intensity) for each residue with respect to the time of the acquisition. The percent exchanged data points for each residue were then fitted to a one phase dissociation curve to obtain the rates of exchange. The standard error from the duplicate experiment was determined by the Graphpad package. The rates of intrinsic hydrolysis evaluated by the real-time NMR method were 50-fold slower than rates of SOS-mediated exchange and consequently not considered for the calculation of the exchange rate.

Computational Modeling of Ubiquitinated KRAS using Rosetta. Conformational flexibility of ubiquitin conjugated to K104 on RAS was analyzed using the UBQ_Gp_LYX-Cterm protocol (Baker et al., 2013) in the Rosetta molecular modeling suite (Leaver-Fay et al., 2011). Briefly, this protocol forms a isopeptide linkage between the specified lysine and the C-terminus of ubiquitin and then samples the orientation of the conjugated ubiquitin by perturbing the torsion angles at the site of conjugation site and several of the residues in the ubiquitin tail, specified in the options by the user. The command to run the executable and the appropriate flags are included in the supplemental flag file. Five thousand models were generated and the lowest scoring 20 are depicted in Figure 5. The low scoring structures did not converge on a single solution and instead produced a variety of models, consistent with the NMR data indicating that ubiquitin remains flexible when conjugated to RAS. We analyzed the lowest scoring 580 models to determine if RAS residues (within 8Å) contact ubiquitin using the features reporter application in Rosetta (Leaver-Fay et al., 2013). To normalize the data, we plotted the percentage of structures that show ubiquitin contacts with RAS (Figure 5). A similar approach was used to model the mUbKRAS[104]-SOS complex using the RAS-SOS structure (PDB: 1BKD) as a starting point. We analyzed the PBD for RAS structures by querying the sequence of KRAS and excluding structures below the e-value cut-off of $2 \times e^{-78}$. Using Rosetta features reporter to search the hydrogen bonds between D69-R102, we

analyzed the 336 PDB entries of RAS containing 536 chains bound to GDP or GTP analogue, in which 206 chains are of RAS bound to GDP and 330 chains contain RAS bound to GTP analogues.

Molecular Dynamics Simulation Analysis of Mono-ubiquitinated KRAS. The crystal structure of the G-domain of wild type KRAS (residue 1-166; PDB: 5UK9) was used as the starting structure for molecular dynamics (MD) simulations of GDP-bound mUbKRAS[104] and WT KRAS. The missing residues, 61 and 64, were modeled in based on the a wild type HRAS structure (PDB: 1QRA) using MODELLER(Webb and Sali, 2016). To simulate mUbKRAS[104] using the CHARMM force field, we created an isopeptide bond between KRAS and ubiquitin by first defining modified lysine (LYQ) and glycine (GLQ) residues. In LYQ, the lysine side chain NH2 atoms were replaced by backbone NH atoms and the residual positive charge on the HZ2 atom was distributed to the neighboring ε-CH2 atoms, resulting in a net charge of zero. To generate GLQ, a covalent bond was defined between the carboxyl terminal carbon and the side-chain NH of LYQ. The new parameters for LYQ and GLQ are provided in supplementary information. Ubiquitin (PDB ID: 1UBQ) and KRAS were then ligated using GROMACS via an isopeptide bond by connecting GLQ76 of ubiquitin and LYQ104 of KRAS after placing the carboxyl terminus carbon atom of GLQ76 within 1.3 Å of the NZ of LYQ104 using UCSF-Chimera (Pettersen et al., 2004). With this approach, two initial configurations of mUbKRAS[104] with Ubiquitin and KRAS in different relative orientations was generated.

Following model building, 1μs-long simulations were performed on the two different conformations of mUbKRAS[104]-GDP. For reference, two independent simulations on WT KRAS-bound to GDP were performed. Each system contained the Mg^{2+} ion as found in the X-ray structure and was solvated with TIP3P water molecules with the ionic strength maintained at 0.15 M by adding Na^+ and Cl^- ions. As mUbKRAS[104] was anticipated to undergo large conformational changes, a minimum of 20 Å between the protein and the edge of the box in order to minimize boundary effects was used. The final system size was 79478 and 81633 atoms for the two mUbKRAS[104] systems and 20518 atoms for WT KRAS. Each system was energy minimized using the steepest decent method setting Fmax to 1000 kJ/mol/nm, and equilibrated using the NVT (constant number of particles, volume and temperature) ensemble at 310K for 100 ps, with a harmonic restraint of force constant 1000 $kJ/mol/nm^2$ applied on the protein and GDP heavy atoms and Mg^{2+}. This was followed by four-1 ns equilibration steps using the isothermal-isobaric (NPT) ensemble while reducing the restraint force constant to 1000, 200, 40 and 0 $kJ/mol/nm^2$, respectively. For each system, the equilibrated configuration was used to run a production phase of 1000 ns using a time step of 2 fs. A constant pressure of 1 bar was employed using the Parrinello-Rahman barostat and a constant temperature of 310K using the Nose-Hoover thermostat. Long-range electrostatic interactions were calculated using the Particle-Mesh Ewald method with the cutoff set to 12 Å, and using the LINCS algorithm to restrain covalent bonds involving hydrogen atoms. The CHARMM36 force field (Best et al., 2012) and GROMACS (v2016.3) were used for all simulations (Abraham et al., 2015).

We evaluated the conformational space sampled by mUbKRAS[104] using the radius of gyration of mUbKRAS[104], the angle defined by the center-of-mass of the Cα atoms of ubiquitin, LYQ104 and KRAS, and residue contacts between KRAS and ubiquitin. Contact is defined to exist if any heavy atom of a residue in one protein is within 4.5 Å of any heavy atom of a residue in the other protein. We also calculated backbone root-mean square fluctuations (RMSF) of residues, and changes in RMSF (δRMSF) in KRAS residues due to ubiquitination as δRMSF = RMSF(mUbKRAS[104]) - RMSF(WT KRAS). Secondary structure content of KRAS helices H2 and H3 and hydrogen bond network evaluated using VMD (Humphrey et al., 1996).

Data file S1. Topology parameters

Topology parameters for modified Lysine (LYQ) and glycine (GLQ) residues for the mUbKRAS[104] isopeptide linkage between KRAS LYQ104 and ubiquitin GLQ76 [4], Related to Figure 5.

```
[ LYQ ]
  [ atoms ]
          N    NH1   -0.470  0
          HN     H    0.310  1
```

```
        CA    CT1    0.070  2
        HA    HB1    0.090  3
        CB    CT2   -0.180  4
       HB1    HA2    0.090  5
       HB2    HA2    0.090  6
        CG    CT2   -0.180  7
       HG1    HA2    0.090  8
       HG2    HA2    0.090  9
        CD    CT2   -0.180 10
       HD1    HA2    0.090 11
       HD2    HA2    0.090 12
        CE    CT2   -0.100 13
       HE1    HA2    0.130 14
       HE2    HA2    0.130 15
        NZ    NH1   -0.470 16
        HZ     H     0.310 17
         C     C     0.510 18
         O     O    -0.510 19
[ bonds ]
        CB    CA
        CG    CB
        CD    CG
        CE    CD
        NZ    CE
         N    HN
         N    CA
         C    CA
         C    +N
        CA    HA
        CB    HB1
        CB    HB2
        CG    HG1
        CG    HG2
        CD    HD1
        CD    HD2
        CE    HE1
        CE    HE2
        NZ    HZ
         O    C
[ impropers ]
         N    -C     CA    HN
         C    CA     +N     O
[ cmap ]
        -C
```

Supplementary Information

Table S1. SOS^{cat}-mediated nucleotide exchange of KRAS K104 mutants compared to WT KRAS, Related to Figure 1.
(adapted from (Yin et al., 2017))

	WT	K104Q	K104R	K104A

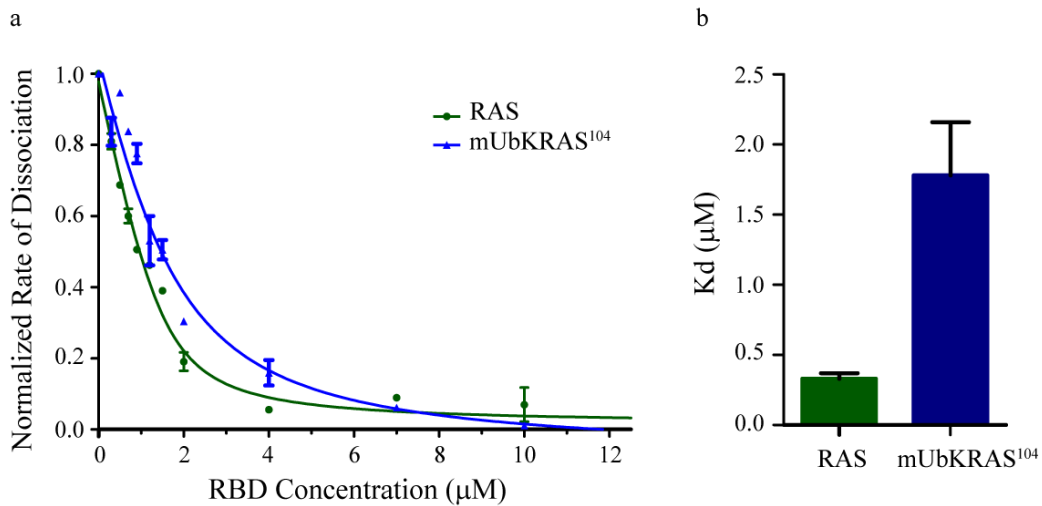|				
Nucleotide exchange rate (10^{-4} s^{-1})	12.5 ± 0.2	2.8 ± 0.1	3.2 ± 0.1	6.3 ± 0.1
Relative exchange Rate	1	0.22	0.26	0.50

Figure S1. Monoubiquitination of KRAS at 104 alters binding to the CRAF RAS binding domain (RBD), Related to Figure 1. a, RAF RBD binding to GMPPNP-bound WT RAS and mUbKRAS[104] was determined by measuring MANT-GMPPNP dissociation as a function of CRAF-RBD concentration using a fluorescence-based assay. b, Binding affinity (Kd) was determined by fitting concentration-dependent dissociation rate. WT RAS binds with 3-fold higher affinity to the CRAF-RBD compared to mUbRas[104]. All measurements were performed in duplicate, results are the mean ± S.D. (n=2).
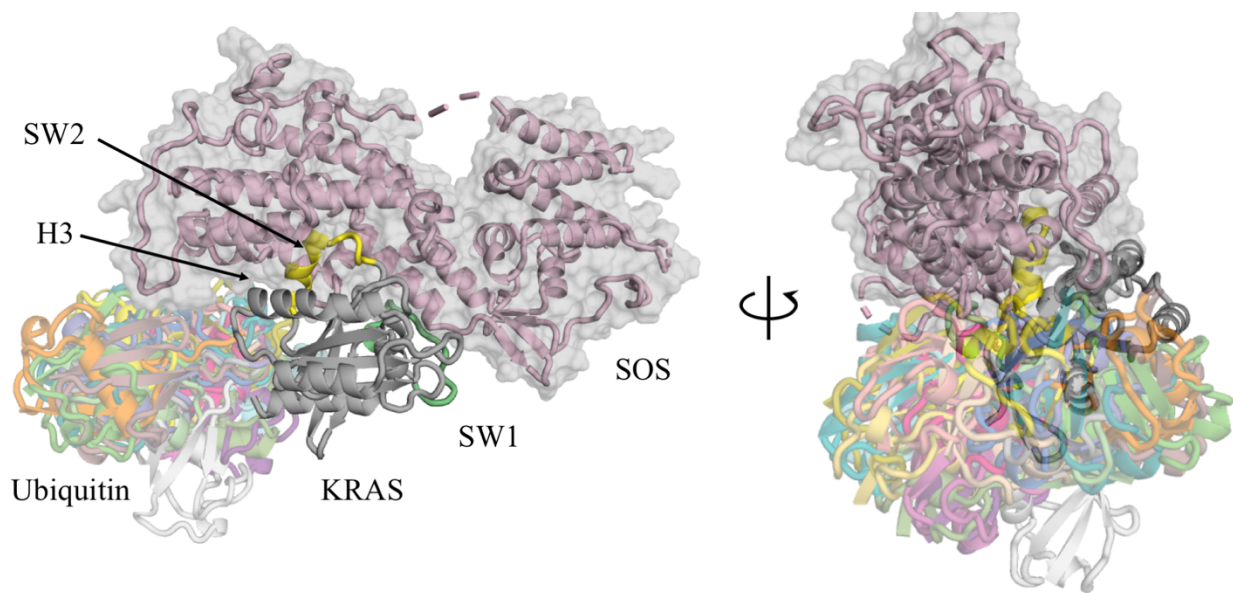
Figure S2. Top 20 Rosetta models of mUbKRAS[104] bound to SOS, using 1BKD as the starting structure, Related to Figure 1. RAS was modeled bound to the SOS catalytic domain. *Left:* side view, *Right;* top. SOS does not significantly perturb ubiquitin conformational freedom. Ubiquitin contacts SOS through a relatively small surface, including intermittent residues in the helix from 884-909 and the loop 1019-1021.
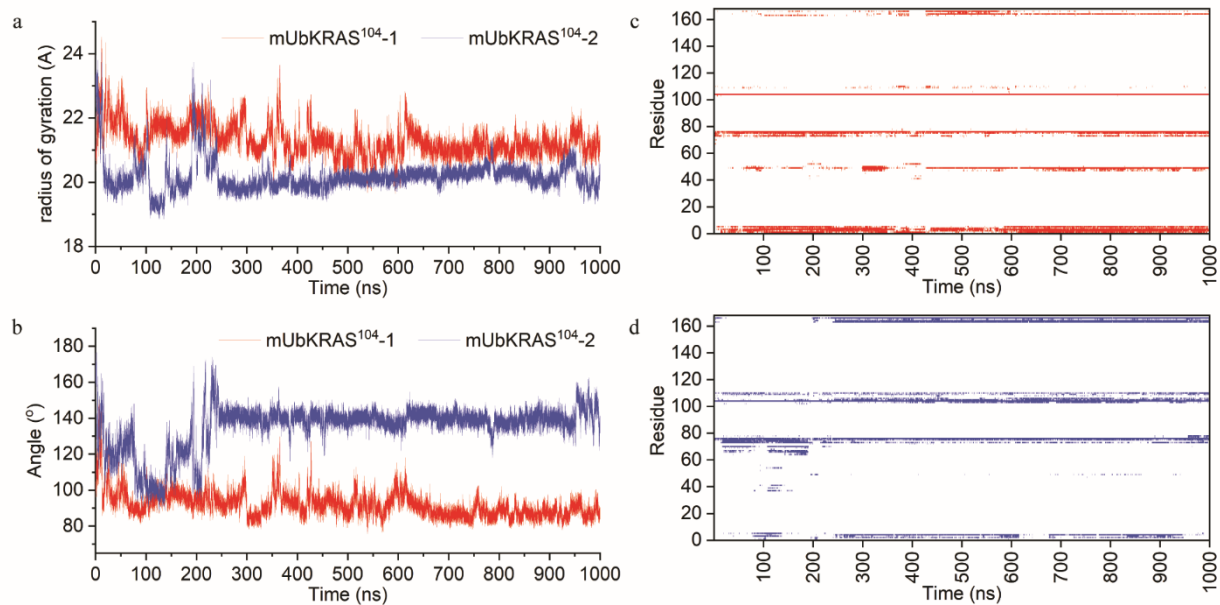
Figure S3. MD simulations of mUbKRAS[104] as a function of phase space, Related to Figure 5. (a) The radius of gyration and (b) angle between vectors defined by the center-of-mass of the Cα atoms of KRAS, LYQ104 and ubiquitin, calculated from two MD runs. The MD runs start from different conformations. mUbKRAS[104] evolves to two different ensembles that do not converge to a single conformation. (c-d) Spontaneous formation of dynamic contacts between KRAS and ubiquitin in simulation 1 (c) and 2 (d).
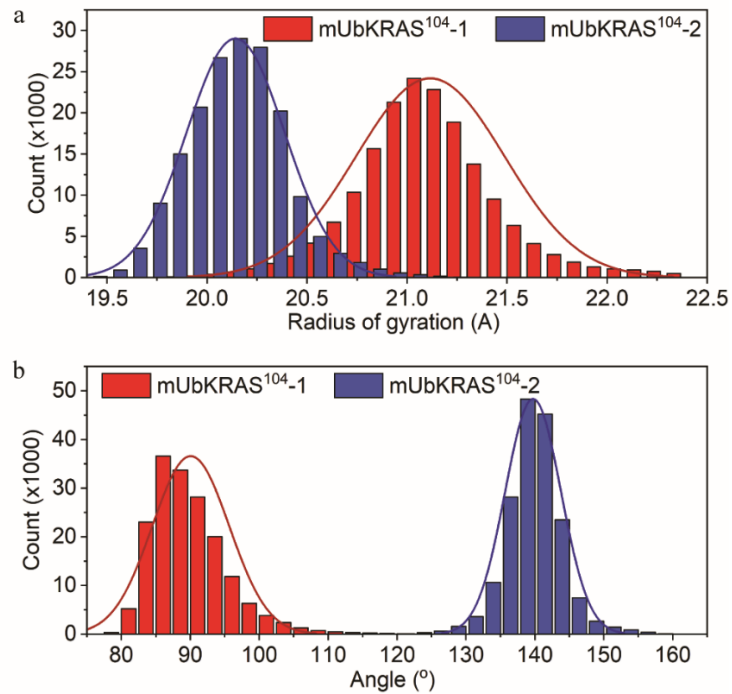
Figure S4. Ubiquitin samples different conformations in two independent MD simulations of mUbKRAS[104], Related to Figure 5. (a) The radius of gyration indicates that conformations in simulation 2 are more compact compared to simulation 1. (b) Ubiquitin is oriented roughly perpendicular to the KRAS-LYQ axis in simulation 1 but not in simulation 2. The data was extracted from the equilibrated portion (last 700 ns) of the MD simulations.
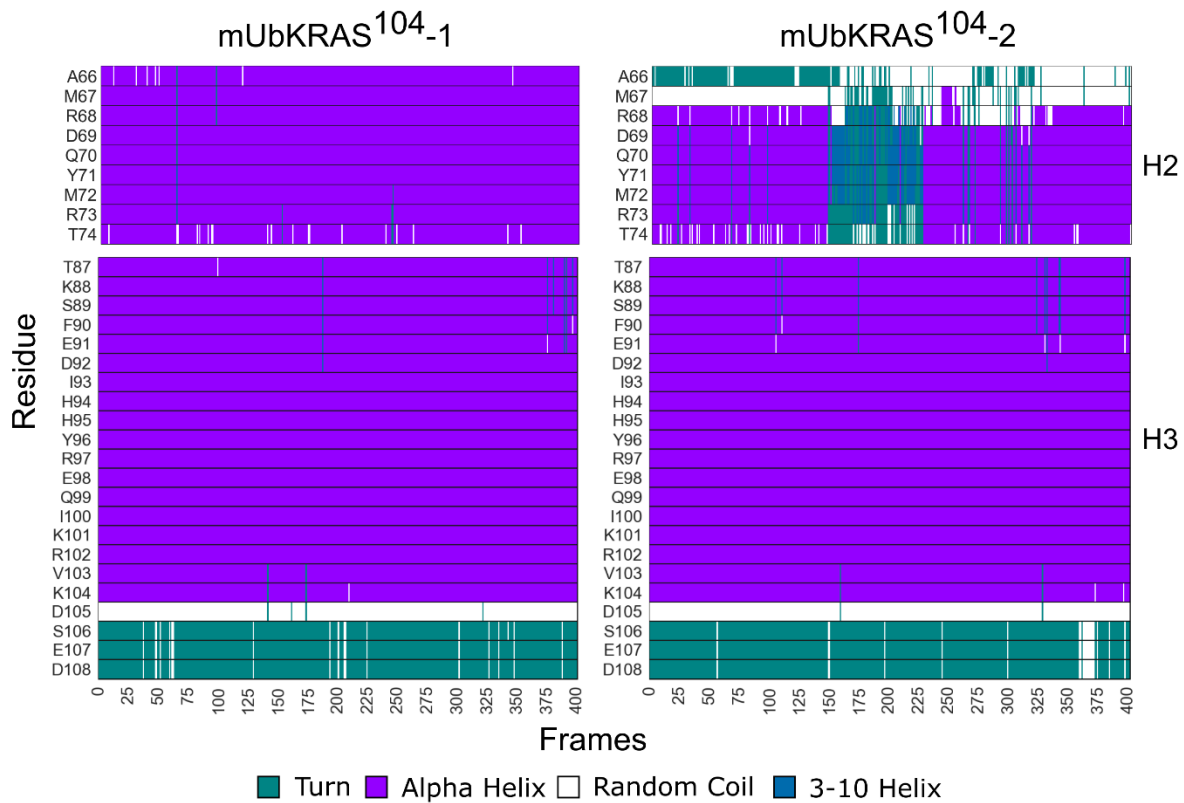
Figure S5. Secondary structure of the H2 and H3 helices over the last 200 ns from two MD simulations of mUbKRAS[104], Related to Figure 5. While H2 and H3 generally remain alpha-helical in both simulations of mUbKRAS[104], H2 is shorter by two amino acids in simulation 2 and its helical content is completely lost in ~20% of the conformers.
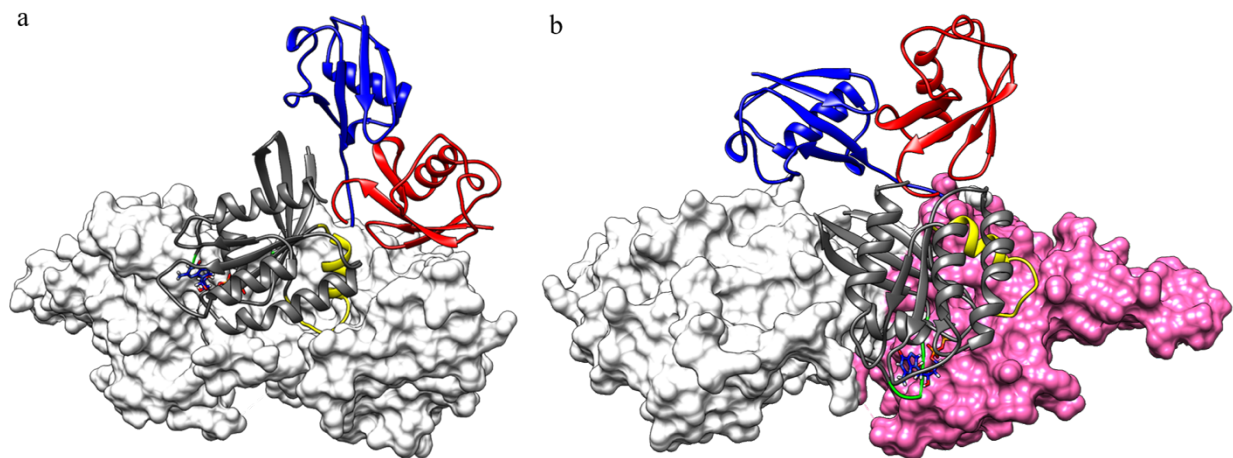
Figure S6. The relative orientation of ubiquitin and KRAS derived from two independent MD runs of mUbKRAS[104]-GDP aligned to (a) apo-RAS (not shown) bound to the SOS catalytic domain and (b) RAS-GMPPNP (not shown) bound to RAS-exchanger Motif (REM) domain (pink) (PDB ID: 1NVW) , Related to Figure 5. SOS is shown in white. KRAS is shown in gray with SWI and SWII in green and yellow, respectively. Representative structures of ubiquitin from simulation 1 and 2 are depicted in red and blue, respectively. The nucleotide is shown as a stick figure.

Reference

Abraham, M.J., Murtola, T., Schulz, R., Páll, S., Smith, J.C., Hess, B., and Lindahl, E. (2015). GROMACS: High performance molecular simulations through multi-level parallelism from laptops to supercomputers. SoftwareX 1–2, 19–25.

Baker, R., Lewis, S.M., Sasaki, A.T., Wilkerson, E.M., Locasale, J.W., Cantley, L.C., Kuhlman, B., Dohlman, H.G., and Campbell, S.L. (2013). Site-specific monoubiquitination activates Ras by impeding GTPase-activating protein function. Nat. Struct. Mol. Biol. 20, 46–52.

Best, R.B., Zhu, X., Shim, J., Lopes, P.E.M., Mittal, J., Feig, M., and MacKerell, A.D. (2012). Optimization of the Additive CHARMM All-Atom Protein Force Field Targeting Improved Sampling of the Backbone ϕ, ψ and Side-Chain $\chi 1$ and $\chi 2$ Dihedral Angles. J. Chem. Theory Comput. 8, 3257–3273.

Humphrey, W., Dalke, A., and Schulten, K. (1996). VMD: visual molecular dynamics. J. Mol. Graph. 14, 33–38, 27–28.

Jung, Y.-S., and Zweckstetter, M. (2004). Mars - robust automatic backbone assignment of proteins. J. Biomol. NMR 30, 11–23.

Leaver-Fay, A., Tyka, M., Lewis, S.M., Lange, O.F., Thompson, J., Jacak, R., Kaufman, K., Renfrew, P.D., Smith, C.A., Sheffler, W., et al. (2011). ROSETTA3: an object-oriented software suite for the simulation and design of macromolecules. Methods Enzymol. 487, 545–574.

Leaver-Fay, A., O'Meara, M.J., Tyka, M., Jacak, R., Song, Y., Kellogg, E.H., Thompson, J., Davis, I.W., Pache, R.A., Lyskov, S., et al. (2013). Scientific benchmarks for guiding macromolecular energy function improvement. Methods Enzymol. 523, 109–143.

Lee, W., Tonelli, M., and Markley, J.L. (2015). NMRFAM-SPARKY: enhanced software for biomolecular NMR spectroscopy. Bioinforma. Oxf. Engl. 31, 1325–1327.

Lenzen, C., Cool, R.H., and Wittinghofer, A. (1995). Analysis of intrinsic and CDC25-stimulated guanine nucleotide exchange of p21ras-nucleotide complexes by fluorescence measurements. Methods Enzymol. 255, 95–109.

Lenzen, C., Cool, R.H., Prinz, H., Kuhlmann, J., and Wittinghofer, A. (1998). Kinetic Analysis by Fluorescence of the Interaction between Ras and the Catalytic Domain of the Guanine Nucleotide Exchange Factor Cdc25Mm. Biochemistry 37, 7420–7430.

Mazhab-Jafari, M.T., Marshall, C.B., Smith, M., Gasmi-Seabrook, G.M.C., Stambolic, V., Rottapel, R., Neel, B.G., and Ikura, M. (2010). Real-time NMR Study of Three Small GTPases Reveals That Fluorescent 2′(3′)-O-(N-Methylanthraniloyl)-tagged Nucleotides Alter Hydrolysis and Exchange Kinetics. J. Biol. Chem. 285, 5132–5136.

Pettersen, E.F., Goddard, T.D., Huang, C.C., Couch, G.S., Greenblatt, D.M., Meng, E.C., and Ferrin, T.E. (2004). UCSF Chimera--a visualization system for exploratory research and analysis. J. Comput. Chem. 25, 1605–1612.

Sondermann, H., Soisson, S.M., Boykevisch, S., Yang, S.-S., Bar-Sagi, D., and Kuriyan, J. (2004). Structural Analysis of Autoinhibition in the Ras Activator Son of Sevenless. Cell 119, 393–405.

Tamiola, K., Acar, B., and Mulder, F.A.A. (2010). Sequence-Specific Random Coil Chemical Shifts of Intrinsically Disordered Proteins. J. Am. Chem. Soc. 132, 18000–18003.

Webb, B., and Sali, A. (2016). Comparative Protein Structure Modeling Using MODELLER. Curr. Protoc. Bioinforma. 54, 5.6.1-5.6.37.

Yin, G., Kistler, S., George, S.D., Kuhlmann, N., Garvey, L., Huynh, M., Bagni, R.K., Lammers, M., Der, C.J., and Campbell, S.L. (2017). A KRAS GTPase K104Q Mutant Retains Downstream Signaling by Offsetting Defects in Regulation. J. Biol. Chem. 292, 4446–4456.